



Tomas Bata University in Zlín
Faculty of Technology

Doctoral Thesis Summary

**Role of Powder Characteristics in Metal Injection
Molding Process**

**Úloha morfologie kovových prášků v procesu
jejich zpracování vstřikováním**

Author: **Mukunda Bhimasena Rao Nagaraj, Ph.D.**

Study program: P3909 Process Engineering

Field of study: 3909V013 Tools and Processes

Supervisor: prof. Ing. Berenika Hausnerová, Ph.D.

External examiners: prof. Ing. Ivan Hudec, PhD
prof. Ing. Jarmila Vilčáková, Ph.D

Zlín, 2024

©Mukunda Bhimasena Rao Nagaraj

Published by **Tomas Bata University in Zlín** in the Edition **Doctoral Thesis Summary**.

The publication was issued in the year 2024

Keywords: metal injection molding, feedstock, particle size distribution, particle shape, particle volume fraction

Klíčová slova v češtině: vstřikování kovových prášků, směs, distribuce velikosti částic, tvar částic, obsah prášku

Full text of the doctoral thesis is available in the Library of the Tomas Bata University in Zlín.

ISBN 978-80-7678-251-8

Resume

Metal powders play a significant role in the success of precision component manufacturing via metal injection molding (MIM). Key metal powder characteristics, such as the particle size distribution and particle shape, dictate the process parameters and component characteristics. This Ph.D. thesis focuses on addressing the simultaneous effects of the above key powder characteristics on feedstock performance in the MIM process. Metal powders with particle size distributions in the range of (3-20) μm , prepared using two widely used fabrication technologies, gas and water atomization, were chosen in the present thesis work. Gas atomization produces spherical particles, whereas water atomization generates irregularly shaped particles. The powders with different sizes and shapes were analyzed for critical solid loading, rheology including flow instabilities, injection molding, and sintering to assess the size and shape effects in MIM. As the majority of the work emphasizes interpreting the shape of the powder particle using a qualitative microscopic technique, a quantitative approach based on the Euclidean distance mapping was developed, and the results were compared with the commercially available dynamic image analyzer.

Resumé (in Czech)

Morfologie kovových prášků hraje významnou roli při vstřikování vysoce plněných práškových materiálů (MIM z *angl.* Metal Injection Molding). Klíčové vlastnosti kovového prášku, jako je distribuce velikostí částic a tvar částic, určují parametry procesu a vlastnosti vyráběných komponent. Tato doktorská práce se zaměřuje na vliv těchto klíčových charakteristik prášku na zpracovatelnost MIM materiálů. V práci byly hodnoceny kovové prášky s rozdílnou distribucí velikostí částic v rozmezí (3-20) μm , připravené pomocí dvou široce používaných výrobních technologií, atomizace plynem a vodou. Atomizace plynem vytváří kulovité částice, zatímco atomizace vodou vytváří částice nepravidelného tvaru. Prášky s různými velikostmi a tvary byly analyzovány v souvislosti s kritickým plněním, reologií včetně nestabilit toku, vstřikováním a slinováním. Jelikož z výsledků vyplývá důležitost interpretace tvaru prášků, byl též vyvinut kvantitativní přístup založený na euklidovském mapování, a výsledky kvantifikace byly porovnány s komerčně dostupnou dynamickou obrazovou analýzou.

ABSTRACT

Metal Injection Molding (MIM) is a high-volume production technology used to manufacture highly precise, nearly net shape, and complex-shaped metal components. The MIM process inherits the shape-making and mass-production capabilities of plastic injection molding along with sintering technology from powder metallurgy.

This thesis presents the significance of powder characteristics, such as particle size distribution and particle shape, in MIM. The physical characteristics of the powders were obtained using a pycnometer, tap density tester, BET surface area analyzer, and particle size analyzer. The shape parameters were derived using a dynamic image analyzer and an in-house analytical tool. The aim of the present thesis is to distinguish the role of particle size distribution and particle shape of gas- and water-atomized powders on MIM processing in terms of maximum or critical solid loading, feedstock flow instabilities, and rheological properties, including wall slip. Considering the above aspects, stainless steel 17-4PH and Co-Cr-Mo-Si gas and water atomized powders were chosen with varying particle size distributions and shapes. The chosen powders were admixed into a wax and high-density polyethylene binder system. Feedstock flow properties were evaluated using a capillary rheometer. It was found that for coarser particles, processability in terms of viscosity is more suitable in the case of gas-atomized powders, whereas in the case of fine powders, water-atomized powders showed higher performance. This finding has not been reported heretofore. Wall slip, as another critical flow parameter, was also found to vary significantly with the size and shape of the powders; round-shaped and large-sized particles promote wall slippage during molding.

The variation in feedstock viscosity with particle size distribution was more pronounced in the case of water-atomized powders (irregular shape) than in gas-atomized powders (spherical) when tested at a constant solid loading. Hence, this study was extended to interpret the role of particle size fractions in different water-atomized powders. Even slight differences in size fractions along with powder shape, which were quantified using shape factor analysis, showed that the feedstocks with higher amounts of coarser fractions with more irregular shapes resulted in higher viscosity, flow instabilities, lower sintered density, and dimensional variations.

CONTENT

1.	Theoretical background	1
1.1	Introduction to metal injection molding	1
1.2	Powder manufacturing and characteristics	2
2.	Aim of the work	4
3.	Results and discussion	5
3.1	Characteristics of gas and water atomized powders	5
3.2	Critical solid loading	7
3.3	Flow behavior affected by powder size and shape	9
3.4	Particle size fraction effect on dimensional stability	12
3.5	Quantification of particle shape	17
5.	Conclusion	20
6.	Contribution to science and practice	21
	References	23
	List of Symbols and Abbreviations	26
	Curriculum Vitae	27
	List of papers and conference presentations	28

1 Theoretical background

1.1 Introduction to metal injection molding

Metal Injection Molding (MIM) is an advanced manufacturing technology that produces highly intricate complex-shaped metal components. MIM technology is competitive with conventional manufacturing technologies, such as powder metallurgy, precision machining, investment casting, and die casting processes, in terms of cost, complexity, and productivity. The mass production of highly precise and complex-shaped metal components with multiple cavities in the tool, lower cycle time during injection molding, and faster debinding and sintering make MIM more viable for industrial applications.

The key advantages of MIM include the shape-making capabilities of a wide range of materials from low-alloy steels, stainless steels, high-temperature alloys, high-wear-resistant alloys, and reactive and refractory materials. The shape-making ability of expensive reactive metals such as titanium and hard metals such as tungsten and other heavy alloys makes it more cost-effective with no material wastage, unlike precision machining techniques. Powder-making capabilities through gas atomization, water atomization, plasma atomization, and chemical processes enable powder producers to manufacture powders with specific particle size distributions, powder morphologies, and chemistry for MIM. Eventually, the powders are mixed with proprietary binder ingredients to produce commercially available MIM feedstocks [1-4].

Metal injection molding (MIM) involves the following critical steps [5-8].

- a) Feedstock preparation or mixing: Fine metal powders are mixed with a polymer binder in appropriate proportions to develop a mixture called a feedstock. Feedstock in granule or pellet form is fed during the next process, injection molding.
- b) Injection molding: The feedstock is heated inside the barrel at appropriate temperatures to form a viscous slurry and injection molded at the optimized temperature, pressure, and speed to form so called *green* part.
- c) Debinding: Part of the binder system or primary binders are removed either through solvent, catalytic or thermal debinding to get so called *brown* part. The remaining brown part then contain connected pores that enable easier evacuation of the remaining binder during following thermal decomposition or thermal debinding.
- d) Sintering: The brown part is densified at elevated temperatures during sintering to obtain a sintered product with the almost no porosity, and mechanical properties comparable with wrought metal. Majority of the materials established in MIM can

attain minimum 97-99% of the theoretical density during sintering enabling better mechanical properties with dimensional consistency.

Any material available in the fine powder form can be successfully used in MIM. The MIM industry has grown significantly, especially in the past decade, owing to the development of multiple materials. Various types of steel (MIM 4605, MIM 4140, MIM 8620, MIM 9310, etc.), stainless steel (MIM SS 316, MIM SS 17-4PH, SS 420, etc.), magnetic materials (MIM Fe-3%Si, MIM Fe-50% Ni etc.), high-temperature alloys (MIM HK30, MIM Nimonic 90, MIM T-400), and tool steels (MIM S-7, MIM M2, etc.), tungsten alloys (W-Co, W-Ni-Fe etc..) and titanium (Cp Ti, Ti-6Al4V) are widely used in industry today.

Stainless steels are ferrous alloys containing at least 12 wt. % chromium. These alloys are categorized based on their main phases as austenitic, ferritic, martensitic, and semi-austenitic. The precipitation-hardened martensitic stainless steel range from 12-17 to wt. % chromium, 4 to 8% nickel, and 0 to 4 wt.% copper with possible additions of molybdenum, silicon, manganese, titanium, and niobium. Of these, 17-4PH is the most popular alloy and also carries identifications such as UNS S17400, AISI 630, ASTM A564, MIM-17-4PH, and AMS 5643. The applications of SS 17-4PH arise from a combination of strength, hardness, and corrosion resistance. Hence, it is widely used in aerospace, medical, automotive, military, and consumer applications [9].

MIM T-400 or Cobalt 400 (Co-Cr-Mo-Si alloy) is a superalloy proven for automotive and aerospace applications (gas turbines) because of its high-temperature wear and corrosion resistance. It contains a hard intermetallic phase dispersed in a matrix of eutectic or solid solution, inducing high wear resistance properties, unlike the formation of carbides. However, the brittle nature of intermetallic phases restricts their use in a wide range of applications [10]. Cobalt 400 is a non-magnetic, excellent corrosion- and high-temperature wear-resistant material used in commercial vehicle applications.

1.2 Powders manufacturing and characteristics

The techniques used to produce metal powders are mechanical techniques, electrolytic techniques, oxide reduction and reaction techniques, and atomization. ground into a small powder. In the last few decades, atomization techniques have replaced other powder production approaches [11-15]. During atomization, melt streams are transformed into liquid or spray droplets in gas, water, or vacuum environments. The gas atomization process produces spherical particles, whereas irregularly shaped particles are produced in the water atomization process. In the gas atomization process, the metal liquids flow down through a refractory metal

nozzle and are atomized into molten metal droplets by high-pressure inert gas flow. Finally, the molten drops solidified into spherical particles while falling into an inert gas chamber. In the water atomization process, high-pressure fluid jets break up a molten metal stream into droplets that solidify into fine irregular powders [2,16].

Powder characteristics, such as particle size distribution and particle shape, are important factors at each stage of the MIM process. Usually, particle sizes ranging from 0.5-20 μm with a mean particle size of $\sim 8 \mu\text{m}$ are suitable for the MIM process [2,14]. Finer powders are detrimental to feedstock homogeneity and injection molding of complex profiles owing to agglomerates in the powder, although it is expected to improve the densification and shape retention during sintering. However, the coarser powders may have defects in the parts produced through injection molding, with lower densification and higher deformation during sintering.

Generally, both gas- or water-atomized powders in MIM can achieve the desired densification and mechanical properties. However, the spherical morphology of the gas-atomized powder enabled packing at a higher density with low post-sintering shrinkage compared to the water-atomized powder. Water-atomized powders are economical and can improve final shape retention during sintering. A higher packing density in the gas-atomized powder can enhance the sintered density and mechanical properties. The oxygen content in the powder dampers densification along with the ductility and corrosion properties [17-19]. The oxygen content is higher in the water-atomized powder (up to 6000 ppm) compared to 600-800 ppm in the gas-atomized powder.

Along with improving the densification during sintering, the spherical morphology of the gas-atomized powder eased the flow behavior of the feedstock and helped fill intricate, complex profiles during injection molding in MIM. The major disadvantage of spherical powder morphology is the reduction in the component strength after binder removal in comparison to the irregular morphology of water-atomized powder. In contrast, irregularly shaped water-atomized powders exhibit higher resistance to flow owing to the larger interparticle friction. However, the shape retention of the component can be compensated in gas-atomized powder by decreasing the particle size of the powder, which enhances the interparticle contact per unit volume [2, 17, 20, 21]. The addition of a fine powder fraction also increases the feedstock viscosity in MIM, resulting in a decrease in shear sensitivity, along with an effect on the surface finish of the components [14,22].

The apparent density typically decreases as the particle shape becomes less spherical. The low apparent density of the non-spherical particles is due to the higher frictional surface area and non-uniformity of the powder particles during packing.

2 Aim of the work

Regardless of the considerable research attention focused on demonstrating the influence of powder particle distribution and powder mean size, most of them lack the possibility of distinguishing between the effect of the shape and size. Therefore, this thesis focuses on spherical and irregular stainless steel (SS) 17-4PH and Co-Cr-Mo-Si (Cobalt 400) powders with varying particle size distributions to determine their effect on MIM processability in terms of critical solid loading, rheological properties, injection molding behavior, dimensional stability, and metallurgical and mechanical properties after sintering.

The powders utilized in this thesis are derived from powder atomization techniques such as gas and water atomization. All the chosen powder combinations in this thesis were admixed with a thermoplastic binder system in a torque compounder. As per the previous work performed by various research scholars, the influence of powder characteristics on rheology and processing in MIM has been widely investigated; however, to the best of our knowledge, none of them simultaneously considered a wide range of particle size distributions (from finer to coarser) and particle shapes (spherical to irregular) to address the size/shape effects in MIM at the time of topic selection. The focus of this work is also the development of a bimodal feedstock combination with a chosen particle size distribution in SS 17-4PH powder using the interparticle spacing/lubricating liquid concept.

Interestingly, few studies have been published on tailoring the particle size and shape fractions for successful injection molding to produce defect-free components with superior post-sintering properties, including dimensional tolerance, in MIM. In this thesis, we attempt to interpret the importance of tailor-making particle size fractions to manufacture defect-free injection-molded and sintered components in MIM.

The present thesis emphasizes the importance of quantitative evaluation of powder morphology, which influences the rheological, injection molding, and sintered properties of MIM. Therefore, the shape of the gas (spherical) and water (irregular) atomized powders will be analyzed using various imaging approaches, and the shape parameters are related to the critical solid loading and rheological, metallurgical, and mechanical properties to investigate the performance of manufacturing highly precise metal components in the MIM industry.

3 Results and discussion

This thesis represents a collection of thematically arranged papers devoted to the aim of the doctoral work:

P-I B. Hausnerova, B.N. Mukund, D. Sanetnik, Rheological Properties of gas and water atomized 17-4PH stainless steel MIM feedstocks: Effect of powder shape and size. Powder Technology 312, (2017) pp. 152-158

P-II B.N. Mukund, B. Hausnerova, Variation in particle size fraction to optimize metal injection molding of water atomized 174-PH stainless steel feedstock. Powder Technology 368 (2020) pp. 130-136

P-III D. Sanetnik, B. Hausnerova, M. Novak, B.N. Mukund, Effect of Particle Size and Shape on Wall Slip of Highly Filled Powder Feedstocks for Material Extrusion and Powder Injection Molding. 3D Printing and Additive Manufacturing 10 (2023) pp.236-244.

P-IV B.N. Mukund, B. Hausnerova, P. Ponizil, Quantification of shape parameters of Co-Cr-Mo-Si alloy powder and their role in the processing of metal injection molding feedstocks. Journal of Manufacturing Processes – submitted in August 2023

In the following the main results obtained and published will be briefly discussed.

3.1 Characteristics of gas and water atomized powders

Our study on bimodal powder combination [13] resulted in a higher packing density for gas-atomized powders with mean particle sizes of (3.3-45) μm . The improved packing density largely depended on the particle-size ratio. The larger the particle size ratio, the higher is the packing density for any composition. Among the three different experimental weight fractions of bimodal combinations the ratio of 75/25 wt.% gives the maximum packing density. This is consistent with the results reported in the literature [23]. The tap density results indicate an increase in packing density with an increase in the number of coarser particles in all bimodal combinations chosen. A bimodal feedstock combination of (6/20) μm , loaded with 70 vol. % of powder also exhibited lowest distortion as well as the highest reproducibility with standard deviation only of (± 0.9) compared to other bimodal combinations chosen. It is evident that the distortion is lower than that of the monodispersed gas-atomized powder (D_{50} :10.8 μm) used in the MIM industry.

In the following, the focus was directed to the simultaneous effect of powder particle size and shape on the processing characteristics in MIM. Eight different gas or water atomized 17-4 PH powders with similar mean particle diameters from 3 to 20 μm were chosen, Figure 1.

The particle size distribution slope parameter, S_w was determined using Equation (1). Generally, a narrower size distribution (S_w of 4-7) of powder tends to result in a higher feedstock viscosity in comparison to powders with a broader size distribution (S_w of 2-4) resulting in lower feedstock viscosity.

$$S_w = \frac{2.56}{\log\left(\frac{D_{90}}{D_{10}}\right)} \quad (1)$$

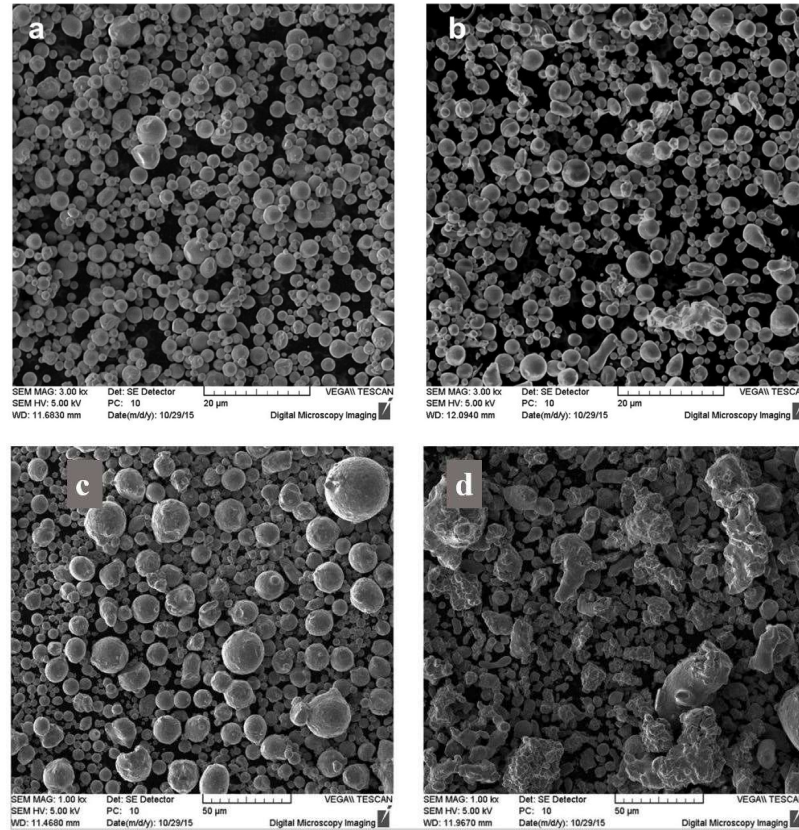


Figure 1 SEM micrographs of SS 17-4PH (a) 3 μm gas atomized powder (b) 3 μm water atomized powder (c) 20 μm gas atomized powder (d) 20 μm water atomized powder [P-I]

The highest values of S_w of 4.90 and 4.88 observed for gas- and water-atomized powders, respectively, with a mean particle diameter of 3 μm , indicating narrower size distributions. The lowest S_w of 2.98 and 3.04 were observed in the case of gas and water, respectively, atomized powders of mean particle size of 20 μm , which might be an indication of easier feedstock mixing and lower feedstock viscosity due to their broader size distribution [2,14].

The spherical powder morphology or shape of the gas-atomized powders has a higher packing density in comparison to the irregular shape in the case of the

respective water-atomized powders. The spherical morphology is expected to exhibit ease of feedstock flow, influencing the filling of complex geometries in injection molding. Powders with finer size distributions tend to form agglomerates, resulting in a lower packing density and higher feedstock viscosity. A lower tap or packing density in water-atomized powders is expected to result in better component strength after binder removal during debinding. This is due to the possible interlocking of powder particles owing to their irregular morphology, which enhances the component strength [2,14,24].

Consequently, finer gas and water atomized powders of 3 μm has higher specific surface area of 0.53 and 0.40 m^2/g , respectively, among the chosen particle size distribution, whereas the coarser particle size of 20 μm was found to have the lowest surface area. The higher the specific surface area of the powder, the higher the resistance to shear deformation (higher viscosity) [25]. Powders with higher specific areas also tend to achieve higher sintered densities, as the surface area drives sintering in MIM [2,26].

It can be observed that 3 μm gas atomized powder had a higher surface area compared to 3 μm water atomized powder. Interestingly, the opposite trend was observed for coarser fractions of water-atomized powder. In this case, the accepted assumption of a higher sintered density with a higher surface area fails for irregularly shaped water-atomized powders. Hence, in the case of finer 3 μm gas- and water-atomized powders, the surface area of the powder drives sintering densification, whereas in the case of coarser water-atomized powders, a higher oxygen content plays a significant role in dictating the sintered density, diminishing the higher surface area effect.

3.2 Critical solid loading

Critical solid loading (CSL) can be measured using the density approach, torque rheometry, and rheological models.

Variation in torque with time observed at high solid loading indicates the proximity of critical solid loading as the binder became locked in the interparticle space, offering more resistivity to the flow. The second method of evaluating the CSL using torque rheometry involves incremental addition and an increase in the solid loading by 1 vol. %. A representative graph of torque analysis indicating higher fluctuation in torque at a powder concentration close to the CSL is shown in Figure 2. At the critical solid loading, the stable torque turns in to highly unstable state with more fluctuations. As can be seen from Table 1, higher CSL was obtained for coarser gas-atomized powders (mean particle sizes of 11 μm and 20 μm) owing to the higher packing density of the powders in the binder matrix. In contrast, water-

atomized powders experienced the opposite trend with a slightly higher CSL obtained in the case of finer 3 μm and 8 μm powders. Hence, in the case of water-atomized powders, the influence of particle size seems to overcome that of particle shape.

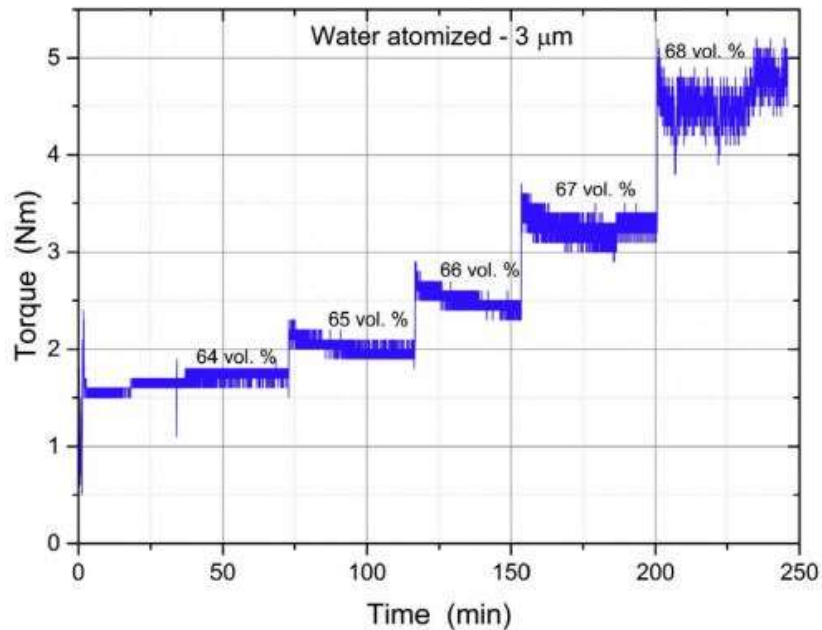


Figure 2 Torque vs. time with an incremental addition of powder indicating critical solid loading (68 vol.%) for a feedstock containing 3 μm SS 17-4PH water atomized powder [P-I]

Table 1 Critical solid loading of SS 17-4PH gas- and water-atomized powders of different particle size range [P-I]

3 μm		8 μm		11 μm		20 μm	
Gas	Water	Gas	Water	Gas	Water	Gas	Water
67	68	66	70	70	66	70	66

Using the density measurement, CSL is derived from the powder concentration value obtained from the theoretical line between the densities of the pure binder and the powder. The third approach involves investigating the CSL in terms of the maximum solid loading parameter using rheological models. However, the models applied to highly filled compounds reveal rather unrealistic values (for more details,

see P-I); thus, the CSL should be determined (similar to industrial practice) from the torque measurements.

3.3 Flow behavior affected by powder size and shape

MIM feedstocks are sensitive to sudden changes in the shear rate during the injection molding of complex profiles. Thus, the evaluation of rheological properties is crucial for optimizing the MIM injection molding process. Feedstock viscosity dictates successful injection molding, which in turn affects the sintered density, dimensional tolerance, and metallurgical properties [2].

As shown in Figure 3, all the chosen gas- and water-atomized feedstocks

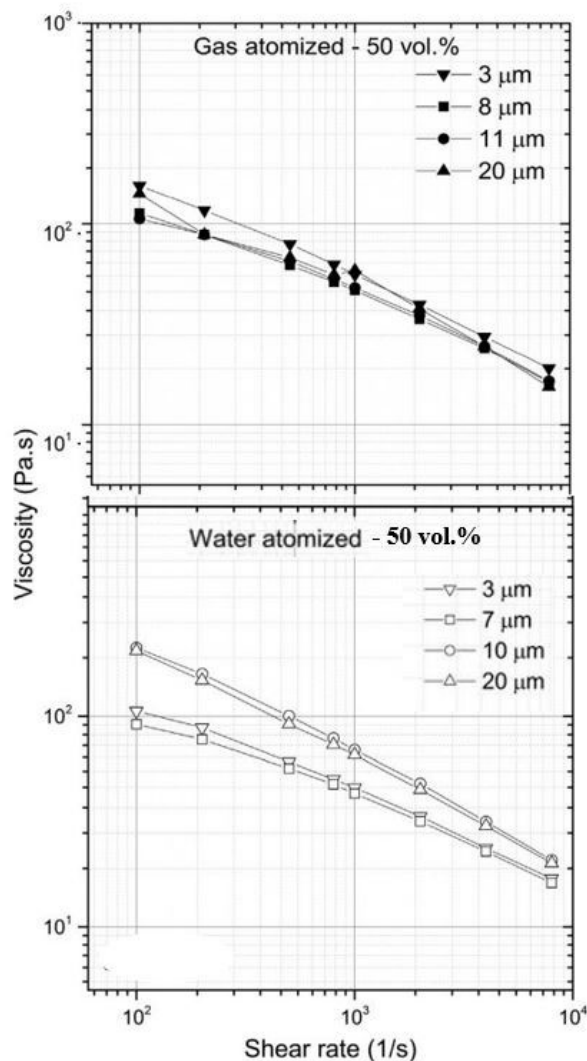


Figure 3 Viscosity as a function of shear rate for the chosen (3-20) μm SS 17-4PH gas and water atomized feedstocks at 50 vol.% solid loading [P-I]

exhibited pseudoplastic behavior with a decrease in viscosity with an increase in shear rate. As expected, the viscosity increased with a decrease in particle size in the gas-atomized powder. However, it can be noted that the differences were negligible, unlike in the case of the water-atomized powder.

Feedstocks containing coarser 20 μm and 10 μm water-atomized powders exhibited significantly higher viscosity with more resistance to flow than the finer 3 μm and 7 μm particle size distributions. This means that for the set of chosen gas and water atomized 3-20 μm mean particle size distributions, higher flowability in the case of coarser particle size distribution fails in the case of water-atomized powder, which is due to its irregular shape. Hence, in the case of the chosen powder size distribution, the powder particle shape significantly influences the feedstock viscosity and overcomes the size because the irregular water-atomized powders exhibit higher viscosity.

The viscosity with respect to solid loading showed fluctuations at lower solids loading (10-30 vol. %) for water-atomized powder. The instabilities were more pronounced in the case of a coarser particle size of 19 μm . A higher solid loading had a stabilizing effect on the flow stability because the powder particles prevent polymer chain disentanglement on the channel wall (P-I).

Wall slip is another flow instability phenomenon that affects the flow properties of MIM feedstock (P-III). It is known that the slip of highly concentrated materials such as MIM feedstocks is connected to the separation of powder and binder, with powder particles migrating to the middle of the flow channel due to the shear rate gradients during processing. Mooney plots showed an increasing tendency toward wall slip with increasing shear stress/pressure observed in the slopes of the fitting lines. Linear fitting lines with coefficients of determination greater than 0.995 were obtained.

The calculated values of the wall slip velocity (Figure 4) show the influence of size and shape on the wall slip phenomena. Feedstocks containing spherical larger particles exhibited higher wall slip velocities in comparison to smaller spherical or irregularly shaped water-atomized powders, indicating that spherical-shaped particles are more prone to wall slip. Spherical particles can rotate more easily upon shearing and hence move to the center of the die, allowing the polymeric binder at the wall. In contrast, water-atomized powders with irregular or flake-like shapes or morphologies tend to orient with the flow front and can resist shearing without losing their uniform distribution within the polymer layer.

In the present study [P-III], it was also observed that flat dies resulted in different wall slip velocities than those obtained with conical dies. The wall slip velocities of all the tested materials at higher shear stresses were lower in conical capillaries than

in flat dies. However, at lower shear stresses, the differences were negligible. Especially, finer particles (3GA) react sensitively to the change in entrance to the capillary dies-at shear stresses about 600 kPa the wall slip velocity was reduced up to 60 % with a conical die.

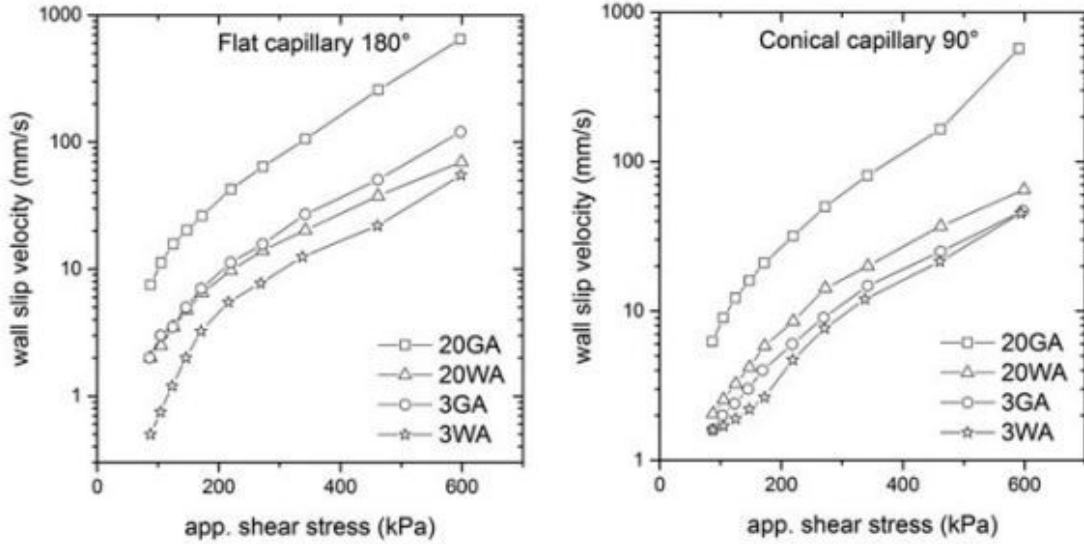


Figure 4 Wall slip velocities of SS 17-4PH feedstocks varying in particle size and shape with various shear stress on flat (entrance angle of 180°) and conical (entrance angle 90°) dies [P-III]

A lower injection speed, conical dies, solid loading near the critical value, and higher viscous melts help to reduce wall slip, and hence, flow instabilities due to powder-binder separation, resulting in defects in the MIM components.

The flow instabilities are due to the smaller interparticle spacing and the low volume fraction of the lubricating liquid causing powder-binder separation in a PIM feedstock [27]. Solid loading influences powder binder separation by correlating the interparticle spacing and the volume fraction of the lubricating liquid. A certain value (0.08) of the volume fraction of the lubricating liquid represents the threshold for powder-binder separation [28].

The segregation of the powder and binder was measured using the interparticle spacing parameter D^i as shown in equation (2). The parameter yields three independent powder characteristics: solid loading (Φ), critical solid loading (Φ_m), and inter particle diameter (D) [101,103,104].

$$D^i = D \left[\left(1 + \frac{1}{\Phi} + \frac{1}{\Phi_m} \right)^{1/3} - 1 \right] \quad (2)$$

It can be noted that the interparticle spacing decreases with mean particle diameter D and increases proportionately with higher particle diameter D for the same loading owing to the increase in critical solid loading (Φ_m) in the latter. Any feedstock with interparticle spacing lower than 0.50 μm and a threshold volume fraction of lubricating liquid of 0.08 is proposed for successful MIM. A bimodal powder combination of (3.3/10.8) μm , (3.3/20) μm and (6/20) μm found to have lowest interparticle spacing of 0.33, 0.21 and 0.35 μm respectively, meeting threshold volume fraction of lubricating liquid exhibiting feedstock stabilities in MIM.

3.4 Particle size fraction effect on dimensional stability

Knowledge of the particle size distribution (PSD) plays a vital role in the production of feedstock and precision engineered metal components in the MIM process. Two powder lots with a similar mean particle size of D_{50} but different D_{90} and D_{10} or vice versa, may result in unacceptable processing performance in MIM. The role of PSD is demonstrated on three microsized SS 17-4PH water-atomized powders with mean particle sizes in the range of 8-9 μm , Table 2 (P-II).

Table 2 Characteristics of 17-4PH stainless steel water atomized powders [P-II]

Powder	D_{10} (μm)	D_{50} (μm)	D_{90} (μm)	ρ_{pycn} (g/cm^3)	ρ_{tap} (g/cm^3)	S_w (-)
WA_24	3.10	7.64	18.90	7.92	4.15	3.26
WA_34	4.18	8.89	18.40	7.90	4.07	3.92
WA_44	4.34	9.13	19.50	7.90	4.05	3.97

Powder abbreviations (WA_24, WA_34, and WA_44) represent the percentage of particles within the size fraction ranging from 10 to 20 μm , as shown in Table 3.

Table 3 Tailored particle size fraction of SS 17-4PH water atomized powders [P-II]

Powder	Particle fraction (%)			
	<5 μm	>5 μm <10 μm	>10 μm <20 μm	>20 μm <35 μm
WA_24	29.93	39.58	23.64	6.85
WA_34	17.45	43.25	33.76	5.54
WA_44	15.19	34.26	43.60	6.95

The particle size fractions between $>20\ \mu\text{m}$ and $<35\ \mu\text{m}$ were similar. All three powders tend to have a round to irregular shape resulting from the water atomization technique: WA_24 powder contains almost 58% of spherical particles with sphericity index of 0.91, whereas WA_34 and WA_44 contain 52% and 41% of spherical particles with sphericities of 0.89 and 0.87, respectively. WA_24, WA_34, and WA_44 powder fractions had aspect ratios of 0.82, 0.80, and 0.76, respectively. Hence, WA_24 contained more spherical particles than WA_34 and WA_44.

A complex-shaped MIM component with a mass of 25 g and dimensions (24 x 43.7 x 20) mm was chosen to investigate the particle size fraction effect of WA_24, WA_34, and WA_44 powders on dimensional consistency in the post-sintering process. The component falls well within the scope of MIM in terms of size and complexity, with multiple holes, slots, and intricate features, as shown in Figure 5. The cross-section varies across the length, enabling an understanding of dimensional stability, including distortion during sintering.

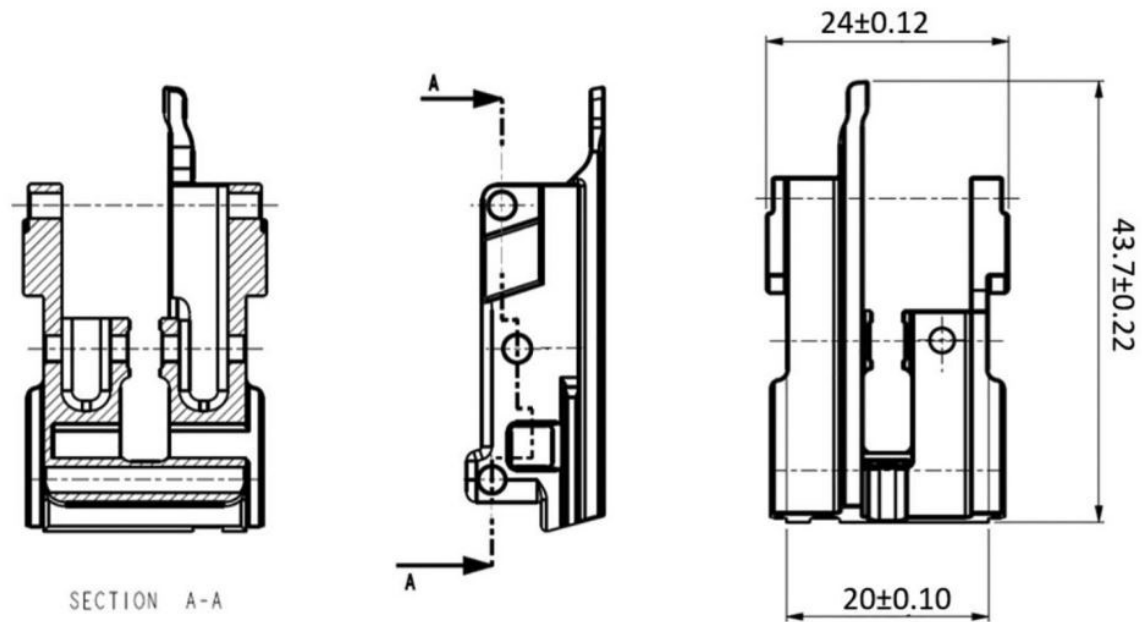


Figure 5 Complex MIM component with functional dimensions [P-II]

Components of the chosen powders were injection-molded and sintered to study their dimensional stability. Figure 5 shows the critical dimensions measured using vernier calipers and micrometers, and the dimensional results are plotted in Figure 6. The effects of the powder size on the dimensional stability of a complex MIM component govern the level of distortion that the material can undergo during sintering. Two critical dimensions related to the slot width (24 ± 0.12) mm (front)

and (20 ± 0.10) mm (back) were inspected to check the dimensional stability or consistency.

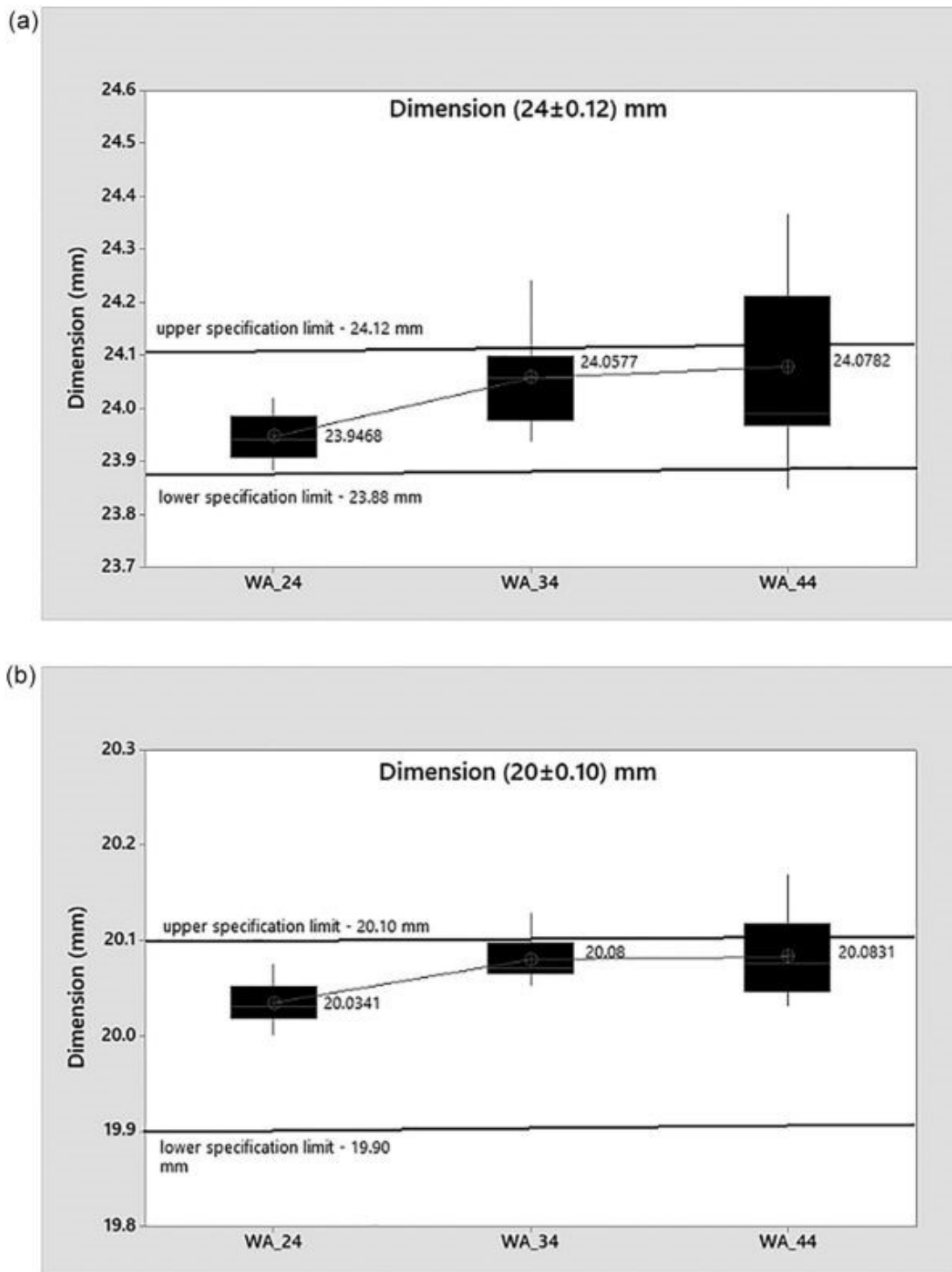


Figure 6 Dimensional variation indicating deformation in WA_24, WA_34 and WA_44 feedstock combination (SS 17-4PH) for the critical dimensions (a) (24 ± 0.12) mm (b) (20 ± 0.1) mm [P-II]

As shown in Figure 6 the components with WA_24 feedstock had dimensions within the specification and well below the achievable tolerance of 1% in MIM [2]. Whereas the components produced from WA_34 and WA_44 exhibited dimensions out of specification limit along with higher standard deviations up to 0.14 and 0.16 mm respectively (for 24 ± 0.12 mm).

The root cause of the higher dimensional variation in WA_34 and WA_44 was investigated by understanding their metallurgical properties. Interestingly, there was no difference in the microstructure and hardness of the parts with the chosen powder-size distribution.

The sintered samples showed the fine martensitic structure of a typical heat-treated SS 17-4PH material. The post-sintering and heat treatment hardness were found to be (28-32 HRC) and (37-41 HRC) respectively, with no particle size effect on the hardness. However, the sintered density was found to have a significant difference with the chosen particle size fractions, as shown in Table 4, despite the absence of surface defects on the parts in both the sintering and post-heat treatment (H900). WA_24 was found to have the highest sintered density of 7.64-7.68 gcm^{-3} whereas lowest density was observed in WA_44 (7.58-7.61 gcm^{-3}).

Table 4 Metallurgical properties of SS 17-4PH water atomized powder fractions chosen [P-II]

Powder	Density (gcm^{-3})	Carbon content (wt%)	Hardness (HRC)
WA_24	7.64–7.68	0.011–0.013	38.8–40.6
WA_34	7.60–7.65	0.019–0.023	38.9–39.7
WA_44	7.58–7.61	0.021–0.028	36.8–39.2

The lower sintered density in WA_44 can be attributed to the inhomogeneities in the feedstock, which exhibit instabilities during viscosity measurements at a constant shear rate test, causing powder-binder separation during injection molding, which could result in density variations in sintering as per the investigation from previous scholars [2,29]. Also, inhomogeneities in a green body generated during injection molding can also result in crack, distortion, and warpage during debinding and sintering affecting dimensional tolerances [2,14].

All feedstocks exhibited pseudoplastic behavior, with viscosity decreasing with the shear rate at 66 vol. % solid loading. Shear sensitivity or power law index (n) was calculated for feedstock with the chosen particle size fraction and the n values

obtained for the feedstocks are 0.40, 0.44 and 0.46 for WA_24, WA_34, WA_44 respectively. The n values reflect the molecular chain ordering of the binder and particle orientation in the flow direction [22,30]. WA_24 particles seem to orient more easily with the flow than the WA_34 and WA_44 feedstocks.

Generally, critical injection molding parameters include melt and mold temperatures, injection speed, holding pressure and time, switch-over point, and cooling time [14]. The feedstock containing WA_24 powder filled the cavity easily at 180 °C, whereas WA_44 was found to have a short fill in the molded component at the same temperature because the WA_44 feedstock exhibits higher viscosity, which is detrimental for the successful injection molding of the complex geometry [2,30]. Hence, the nozzle temperature was increased incrementally from 180 °C to 195 °C to completely fill the components with the WA_44 compound. All other parameters, such as barrel temperature, holding pressure and time, injection speed, and switch over point (SOP), were kept constant for all feedstocks. The initial metering stroke was maintained at 42 cm³ and the injection screw was moved until the SOP reached 32 cm³ to fill approximately 10 cm³ of the molten material in the cavity of the mold. Filling percentages of the MIM components were 60%, 52%, and 49% for WA_24, WA_34, and WA_44, respectively, in the filling phase, whereas the rest of the components was successfully filled completely in the packing phase. The changeover injection pressure generated during injection molding was found to be significantly higher (897 bar) for WA_44 feedstock compared to 623 and 758 bar generated for WA_24 and WA_34, respectively.

This is attributed to the flow behavior of the feedstock containing the coarser particle fraction (WA_44), which exhibited instabilities during rheological measurements, reflecting structural variation upon shearing. This indicates that the stability of the viscosity, that is, its time dependence, is a more important variable than its variation with the shear rate. The green components produced using the feedstock containing WA_44 had a rough surface compared with the other two feedstocks.

Hence, the reason for the lower sintered density and higher dimensional variation in WA_34 and WA_44 is attributed to the increase in the population of coarser particles with less sphericity or more irregular particle shape, inducing inhomogeneities in the green body, resulting in instability and stress concentration during injection molding, resulting in deformation during sintering. It is desirable to control and tailor the powder characteristics in terms of particle size fractions as well as their shape to produce quality components in MIM.

3.5 Quantification of particle shape

As became clear from the previous chapter, the quantification of powder shapes plays a crucial role in understanding their effect on the process parameters and product characteristics in MIM. In fundamental and applied research, the powder shape is interpreted as either spherical or irregular based on qualitative analysis (scanning electron microscopy). A dynamic image analyzer (DIA) can be used as an accurate measurement technique that provides valuable information on the particle shape parameters [31,32]. The degree of sphericity is an important parameter for the quantitative description of the particle shape.

Particle shape analysis was performed on the Co-Cr-Mo-Si (Cobalt 400) gas (GA) and water-atomized (WA) powders. Table 5 shows the particle size distributions of the GA and WA powders obtained using laser diffraction and a dynamic image analyzer. No significant differences were detected between the PSD resulting from these two methods.

Table 5 Particle size distribution of gas and water atomized Cobalt 400 powders obtained from laser diffraction and dynamic image analyzer [P-IV]

Powder	Laser diffraction			Dynamic image analyzer		
	D_{10} μm	D_{50} μm	D_{90} μm	D_{10} μm	D_{50} μm	D_{90} μm
GA	4.1	8.1	14.0	4.5	9.1	13.8
WA	3.9	8.9	16.3	4.8	9.3	15.1

Gas atomized powders have a higher tap or packing density owing to their spherical morphology compared to the irregular morphology in water atomized powder (Figure 7).

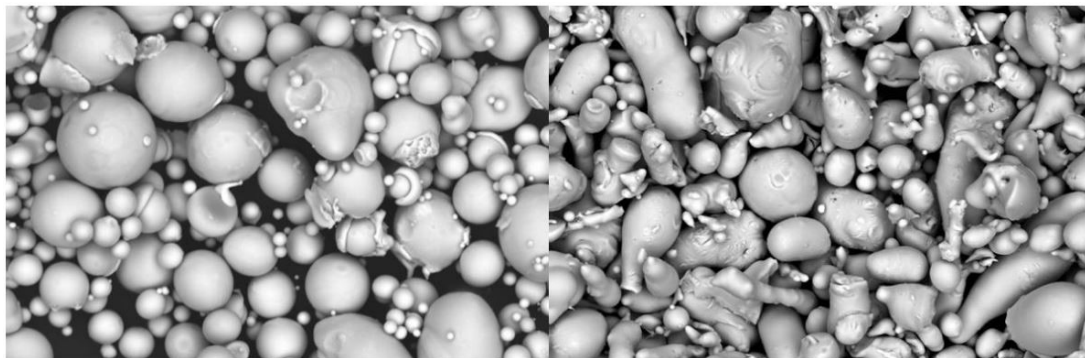


Figure 7 SEM micrographs of gas- (left) and water-atomized (right) Cobalt 400 powders [P-IV]

Particle shapes were first quantified using a dynamic image analyzer. DIA is capable of measuring shape of a powder particle as it passes through a light source by capturing the individual particles using a high-speed digital camera. The powder was conveyed using liquid or gas, and software was used to calculate the 2D shape of the particles. Then, the quantification of particle shape was also proposed using the Euclidean Distance Map (EDM). Figure 8 describes the EDM with the help of the scheme, as interpreted below. First, an original SEM image (a) is transferred to a threshold image (b), which is applied to the grayscale image to reduce image granulation and simplify the following thresholding. Subsequently, all the edge pixels (black pixels with adjacent white pixels) were set to red (c). The Euclidean distance of all white pixels for EDM must be computed to the nearest black pixel. The nearest pixel must be the edge pixel. Computation of the distances of all white pixels to only edge pixels accelerates the image processing, resulting in EDM (d). The Euclidean distance to the nearest edge pixel (red) is computed for any pixel inside the particle (white pixels). A brighter green color corresponds to a greater distance. Local maxima of Euclidean distances are selected as centers of particles (e) under the condition that if more local maxima are found close to each other, the center is set to the total maximum only. When the particles were connected, they were separated by the boundary created at the narrowest position (f).

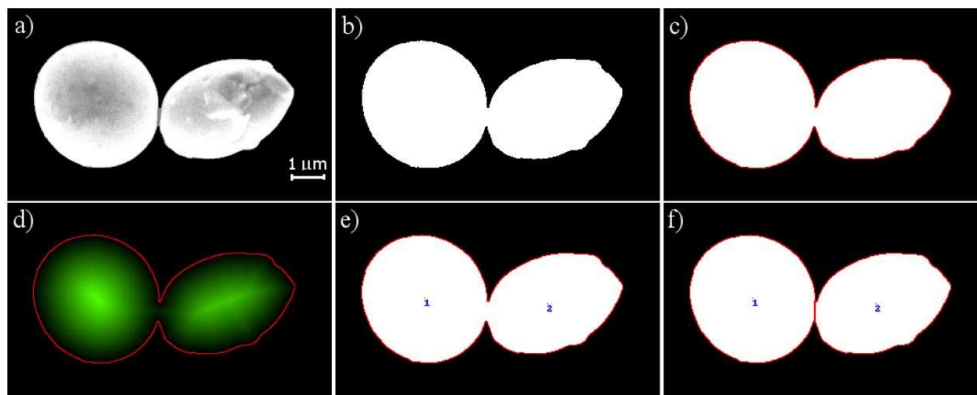


Figure 8 Particle shape analysis via Euclidean Distance Map [P-IV]

Based on the analysis performed using EDM, the shape of the powder was quantified using EDM as:

- Aspect ratio (width/length ratio): ratio of minimal to maximal caliper diameter (w/l). It changes from 0 for a thin rod to 1 for a sphere.

- Symmetry $\frac{1}{2} \left(1 + \min \left(\frac{r_1}{r_2} \right) \right)$ - minimal ratio of r_1 (distance from particle center to boundary) and opposite r_2 . It changed from 1/2 for a thin rod to one for a sphere.
- Circularity $\sqrt{\frac{4\pi A}{U^2}}$, where A is the area of the particle image, and U is its perimeter. It changes from 0 for a thin rod to 1 for a sphere.

Table 6 depicts the comparison of shape parameters (circularity, aspect ratio and symmetry) obtained from both DIA and EDM. As per the DIA, the GA powder has approximately 75.5 vol.% of spherical particles with a circularity of 0.939, whereas the WA powder consists of only 36.5 vol.% of spherical particles with mean circularity of 0.85. WA powder consisted of 98.1 vol. % of particles having an aspect ratio of 0.679 indicating higher irregularity in comparison to GA (0.815 for 80 vol.%) particles. Both DIA and EDM data corresponds well in case of aspect ratio (0.70) for WA powder whereas, GA found to be 0.815 and 0.917 in DIA and EDM respectively. As expected from the spherical morphology in GA, symmetry observed in DIA found to reveal 88 vol.% symmetrical particles with a mean value of 0.921 in comparison to 46.6 vol.% in case of WA powder. EDM results in case of symmetry found to be 0.948 and 0.851 in case of GA and WA respectively. In general, both the methods found to correlate well for the parameters discussed enabling in quantifying the shape of the powders.

Table 6 Comparison of the shape parameters from dynamic image analysis (DIA) and Euclidian distance maps (EDM) methods [P-IV]

Method		DIA		EDM	
		GA	WA	GA	WA
Circularity	Mean	0.939	0.853		
	vol. %	75.5	36.5	0.969±0.004	0.871±0.009
Aspect ratio	Mean	0.815	0.679		
	vol. %	80.2	98.1	0.917±0.004	0.707±0.013
Symmetry	Mean	0.921	0.885		
	vol. %	88.2	46.6	0.948±0.002	0.851±0.007

4 Conclusion

The presented thesis emphasizes the importance of the simultaneous consideration of particle size and shape in the processing of highly complex metal components in metal injection molding MIM. The powder particle size/shape effect derived from the powder manufacturing route has a pronounced effect on the processability of feedstocks. The effect of particle size and shape on the rheology of gas and water atomized feedstocks indicate that coarser (11 and 20 μm) particles favor processability in terms of critical solid loading, viscosity, and mixing torque, whereas fine powders (3 and 8 μm) showed better performance in the case of irregular water-atomized powder. The latter is contrary to the generally accepted statements concerning the effect of particle shape on the flow behavior of MIM feedstocks. For the set of investigated powders ranging in powder particle size distribution from (3-20 μm), the influence of size exceeded that of shape in the case of finer fractions. It is interesting to note that the viscosity changes in the case of water-atomized powders (3-20 μm) are significant when measured at constant solid loading, whereas the difference is negligible for gas-atomized powders.

The significant viscosity changes with particle size distribution in water-atomized powder enable scientists and engineers to carefully control and tailor the particle size fractions, as well as their shape, to produce quality components in MIM. The critical parameters that influence the dimensional stability of MIM components include the particle size distribution, sphericity/aspect ratio of the powder, stability of viscosity, injection molding parameters, and sintering deformation. The increase in the population of the coarser particle fraction along with the relatively irregular shape has a significant influence on the product quality with defects induced during injection molding along with deformation in sintering, leading to dimensional variations.

Quantification of the particle shape plays a crucial role in understanding its effect on MIM processing. An in-house developed approach based on the Euclidian distance mapping provides similar values of symmetry, aspect ratio, and circularity in line with a dynamic image analyzer, a commercially available tool to quantify the shape descriptors of powder particles.

5 Contribution to science and practice

MIM metal component business is estimated to earn ~3 billion USD in revenue in 2022, with an average growth of 15 % by year. The market is projected to reach USD 8-9 billion by 2030. The global MIM market is expected to grow at a significant rate owing to the high cost-effectiveness of MIM technology compared to other manufacturing processes such as machining or investment casting.

Based on the material segmentation, stainless steel is the leading material in 2022 with 50-75 % of the global applications driving the market. Among these, 17-4PH, which is widely used in medical, automotive, military, and consumer electronics applications, has driven growth because of its combination of strength and corrosion properties. However, a better understanding of the role of powder features in the MIM process is essential for designing and optimizing feedstocks and injection molding parameters to produce quality parts.

This PhD thesis focuses on how the influence of key powder characteristics, particle size, and shape simultaneously affects the feedstock performance throughout the process. The findings of this PhD thesis are considered the most important contributions to science and practice:

1. Irregularly shaped fine powders (produced by water atomization) performed better in terms of rheological behavior, whereas spherical coarser powder particles (produced by gas atomization) showed a marked influence on the flow properties. This enabled a global contract manufacturer and an industry leader like Indo MIM to implement irregularly shaped finer powders in mass production of highly intricate, complex MIM geometries that significantly reduced the defects during injection molding (short fill, void, interconnected voids, and distortion) in MIM, enabling an increase in yield up to ~10-20% with significant cost savings.

2. Optimization of feedstock design in terms of powder-binder composition has been a challenge in MIM. Any excess powder or binder in the feedstock may lead to filling of issues/surface defects during injection and distortion of the components during sintering. The window derived from interparticle spacing and volume fraction of lubricating liquid concepts should help in designing feedstocks in consideration of both easier filling in injection molding and better shape retention during sintering. The derived scientific approach was successfully demonstrated on a Cobalt 400 alloy in optimizing the gas and water atomized feedstocks for the successful filling of precision and complex metal components in MIM. This reduces or eliminates the series of trial-and-error iterations during the feedstock design and hence saves both man-hours and the material cost, facilitating a quick turn-around on feedstock optimization in turn material developmental activities.

3. Considerations of the effect of particle size fractions on the dimensional stability in a water-atomized feedstock is a new area in the present thesis. It is necessary to engineer the powder particle size fraction to attain dimensional consistency during the processing of precision metal components in MIM. This PhD thesis highlights the importance of tailoring the powder particle size fraction and particle shape during the manufacturing of powders. Any noticeable variations in powder particle size fractions and shapes could result in flow instabilities during injection molding, affecting the sintering properties, including the dimensional performance of MIM components. This published work (paper II of the thesis work) was acknowledged by “PIM International”, a widely accepted journal in the PIM industrial category, as a recognition of the scientific and industrial community (<https://www.pim-international.com/wp-content/uploads/sites/2/2020/09/Vol-14-No-3.pdf>).

4. It is important to quantify the shape or morphology of the powder particles. The present practice is to understand the particle shape or morphology in MIM through qualitative analysis (SEM). The present thesis emphasizes the derivation of shape parameters such as circularity, aspect ratio, and symmetry quantitatively using DIA, which helps in assessing the shape of the powders. The shape parameters seem to influence the feedstock rheology, injection molding, and sintered metallurgical and mechanical properties in MIM.

5. A new quantification approach based on Euclidian distance mapping (EDM) was developed to evaluate the symmetry, aspect ratio, and circularity of powder particles. This approach helps to measure the particle shape of the powder quantitatively in line with the dynamic image analyzer, a tool available in the market to quantify the shape descriptors.

References

1. D.A. Issitt, P.J. James, Rheology of mixed powder plastisols, *Powder Metallurgy*, 29 (1986) 259-264.
2. R.M. German, A. Bose, *Injection Molding of Metals and Ceramics*, 1997, Metal Powder Industries Federation, Princeton, New Jersey.
3. C. Karatas, A. Kocer, H.I. Aenal, S. Saritas, Rheological properties of feedstocks prepared with steatite powder and polyethylene-based thermoplastic binders, *Journal of Materials Processing Technology*, 152 (2004) 77-83.
4. N. Williams, Global markets for metal injection molding – Data and insight from World PM2022 and beyond, *Powder Injection Molding International*, 16 (2022) 55-62.
5. V.A. Krauss, A.M. Oliveira, A.N. Klein, H.A. Al-Qureshi, M.C. Fredel, A model for PEG removal from alumina injection moulded parts by solvent debinding, *Journal of Materials Processing Technology*, 182 (2007) 268-273.
6. G. Schlieper, G. Dowson, B. Williams, F. Petzoldt, *Metal Injection Moulding*, 2013, Springer-Verlag, Berlin.
7. D. F. Heaney, *Handbook of Metal Injection Molding*, 2012, Woodhead Publishing, Cambridge.
8. R.M. German, Markets applications and financial aspects of global metal powder injection moulding (MIM) technologies. *Metal Powder Report*, 67 (2012) 18-26.
9. R.M. German, MIM 17-4PH Stainless steel: Processing, properties, and best practice, *Powder Injection Molding International*, 12 (2018) 49-76.
10. Kennametal, Stellite alloys, <https://www.stellite.com/us/en/products/stellite-family/stellite-family/tribaloy.html>. accessed 1st December 2023.
11. G. Thavanayagam, K. L. Pickering, J. E. Swan, P. Cao, Analysis of rheological behaviour of titanium feedstocks formulated with a water-soluble binder system for powder injection moulding, *Powder Technology*, 269 (2015) 227–232.
12. W. K. You, J. P. Choi, S. M. Yoon, J. S. Lee, Low temperature powder injection molding of iron micro-nano powder mixture, *Powder Technology*, 228 (2012) 199–205.
13. B. N. Mukund, B. Hausnerova, T. S. Shivashankar, Development of 17-4PH stainless steel bimodal powder injection molding feedstock with the help of interparticle spacing/lubricating liquid concept, *Powder Technology*, 283 (2015) 24–31.
14. D. F. Heaney, *Handbook of Metal Injection Molding*, 2012, Woodhead Publishing, Cambridge.
15. G. Chen, S. Y. Zhao, P. Tan, J. Wang, C. S. Xiang, H. P. Tang, A comparative study of Ti6Al-4V powders for additive manufacturing by gas atomization, plasma rotating electrode process and plasma atomization, *Powder Technology*, 333 (2018) 38-46.

16. R. M. German, *Powder Metallurgy of Iron and Steel*, 1998, John Wiley & Sons, New York
17. R. P. Koseski, P. Suri, N.B. Earhardt, R. M. German, Y. S. Kwon, Microstructural evolution of injection molded gas- and water-atomized 316L stainless steel powder during sintering, *Material Science Engineering A*, 390 (2005) 171–177.
18. K. Yu, S. Ye, W. Mo, Y. Lv, H. Jiang, R. Ma, C. Kwok, P. Yu, Oxygen content control in metal injection molding of 316L austenitic stainless steel using water atomized powder, *Journal of Manufacturing Processes*, 50 (2020) 498-509.
19. A. Mostafaei, J. Toman, E.L. Stevens, E.T. Hughes, Y.L Krimer, M. Chmielus, Microstructural evolution and mechanical properties of differently heat-treated binder jet printed samples from gas- and water-atomized alloy 625 powders, *Acta Materialia*, 124 (2017) 280–289.
20. H. O. Gulsoy, N. Gulsoy, R. Calisici, Particle morphology influence on mechanical and biocompatibility properties of injection molded Ti alloy powder, *Biomedical Materials Engineering*, 24 (2014) 1861-1873.
21. B. Hausnerova, T. Kitano, I. Kuritka, J. Prindis, L. Marcanikova, The role of powder particle size distribution in processability of powder injection molding compounds, *International Journal of Polymer Analysis and Characterization*, 16 (2011) 141–151.
22. M. E. Sotomayor, A. Varez, B. Levenfeld, Influence of powder particle size distribution on rheological properties of 316L powder injection molding feedstock, *Powder Technology*, 200 (2010) 30-36.
23. R. M. German, *Particle Packing Characteristics*, Metal Powder Industries Federation, 1989, Princeton, New Jersey.
24. S. Park, Y. Wu, D. F. Heaney, X. Zou, G. Gai, R. M. German, Rheological and thermal debinding behaviors in titanium powder injection molding, *Metallurgical and Materials Transactions A*, 40 (2009) 215–222.
25. A. V. Shenoy, *Rheology of Filled Polymer Systems*, Kluwer Academic Publishers, 1999, Dordrecht.
26. B. N. Mukund, T. S. Shivashankar, Rheological and Mechanical properties of gas and water atomized SS 17-4PH feedstock used in Metal Injection Molding (MIM), *World Congress on Powder Metallurgy*, 2018, Beijing, China.
27. T. S. Shivashankar, R. K. Enneti, S. J. Park, R. M. German, S. V. Atre, The effects of material attributes on powder–binder separation phenomena in powder injection molding, *Powder Technology*, 243 (2013) 79–84.
28. B. N. Mukund, T. S. Shivashankar, Effect of particle spacing on shape retention phenomena in powder injection molding, *European Powder Metallurgy Association*, 2013, Shrewsbury.
29. L. V. Dihoru, L. N. Smith, R. Orban, R. M. German, *Experimental Study and*

- Neural Network Modelling of the Stability of Powder Injection Molding Feedstock, *Materials and Manufacturing Process*, 15 (2000) 419-438.
30. R. Machaka, P. Ndlangamandla, M. Seerane, Capillary rheological studies of 17-4 PH MIM feedstocks prepared using a custom CSIR binder system, *Powder Technology*, 326 (2018) 37–43.
31. U. Ulusoy, M. Yekeler, Dynamic image analysis of calcite particles created by different mills, *International Journal of Minerals Process*, 133 (2014) 83–90.
32. U. Ulusoy, Quantifying of particle shape differences of differently milled barite using a novel technique: Dynamic image analysis, *Materialia*, 8 (2019) 100434.

List of Symbols and Abbreviations

Symbols

D_{10}	Diameter under which is 10 % of particles
D_{50}	Diameter under which is 50 % of particles
D_{90}	Diameter under which is 90 % of particles
D	Mean particle diameter
v_{slip}	Slip Velocity
v_{true}	True velocity
ϕ	Solid loading
ϕ_m	Critical solid loading
$\dot{\gamma}$	Shear rate
$\dot{\gamma}_a$	Apparent shear rate
η	Material/compound viscosity
$\eta(\dot{\gamma})$	Shear-dependent viscosity
η_0	Zero-shear viscosity
η_a	Apparent viscosity
η_b	Viscosity of the pure binder
η_r	Relative viscosity
τ_a	Apparent shear stress
n	Power law index
S_w	Particle size distribution width slope parameter
T_g	Glass transition temperature
E_a	Activation energy
D_i	Interparticle spacing parameter

Abbreviations

MIM	Metal Injection Molding
PW	Paraffin wax
HDPE	High density polyethylene
LDPE	Low density polyethylene
PW	Paraffin wax
POM	Polyoxymethylene
SS	Stainless steel
GA	Gas atomization
WA	Water atomization
PM	Powder metallurgy
PSD	Particle size distribution
PIM	Powder injection molding
SEM	Scanning electron microscopy
UTS	Ultimate tensile strength
vol%	Volume percentage
wt%	Weight percentage
YS	Yield strength
DIA	Dynamic image analyzer
EDM	Euclidean distance map
SOP	Switch over point

Curriculum Vitae

Personal information

Mukunda Bhimasena Rao Nagaraj

DOB: 01. 01. 1982

Address: 8543 State Highway 151

San Antonio, Texas 78245, USA

Email: rao_nagaraj@utb.cz

Cell Phone: +1 210 557 1594

Education

1999-2004	Bachelor of Engineering. Visvesvaraya Technological University, Belgaum, India
2008 – 2011	Master of Science Visvesvaraya Technological University, Belgaum, India
2017 – 2024	Doctoral Tomas Bata University in Zlin, Faculty of Technology Doctoral study program – Process Engineering Study course –Tools and Processes.

Professional work experience

01/2005-02/2021: Manager-R&D & Technology development,

Indo MIM Pvt Ltd., Bengaluru, India

02/2021–present: Senior Manager & Head - R&D / Additive Manufacturing
Operations, Indo MIM Inc., Texas, USA

Languages

English, Kannada, Hindi

List of papers and conference contributions

B.N. Mukund, G.S. Sevant Kumar, A. Padmanabha, Influence of Powder Parameters on the Properties of Highly Filled Metal Powder Systems. Indian Journal of Advanced Chemical Science 2 (2014) pp. 93 -97.

B.N. Mukund, B. Hausnerova, T.S. Shivashankar, Development of 17-4 PH stainless steel bimodal powder injection molding feedstock with the help of interparticle spacing/lubricating liquid concept, Powder Technology 283 (2015) pp. 24-31

B. Hausnerova, B.N. Mukund, D. Sanetnik, Rheological Properties of gas and water atomized 17-4PH stainless steel MIM feedstocks: Effect of powder shape and size. Powder Technology 312, (2017) pp. 152-158

B.N. Mukund, B. Hausnerova, Variation in particle size fraction to optimize metal injection molding of water atomized 174-PH stainless steel feedstock. Powder Technology 368 (2020) pp. 130-136

D. Sanetnik, B. Hausnerova, M. Novak, B.N. Mukund, Effect of Particle Size and Shape on Wall Slip of Highly Filled Powder Feedstocks for Material Extrusion and Powder Injection Molding. 3D Printing and Additive Manufacturing 10 (2023) pp.236-244.

B.N. Mukund, B. Hausnerova, P. Ponizil, Quantification of shape parameters of Co-Cr-Mo-Si alloy powder and their role in the processing of metal injection molding feedstocks. Journal of Manufacturing Processes – submitted in August 2023

B.N. Mukund, T.S. Shivashankar, Effect of particle spacing on shape retention phenomena in Powder Injection Molding, Euro PM 2013, European Powder metallurgy Association, Euro PM Congress Proceedings, 2013, Gothenburg, Sweden.

B.N. Mukund, G.S. Sevant Kumar, A. Padmanabha, Effect of processing temperature on the separation phenomena in concentrated metal powder suspensions in PIM, AWPP2013, Proceedings of the Asia workshop on polymer processing, 2013, Goa, India.

B.N. Mukund, T.S. Shivashankar, Effect of Bimodal Mixtures on Rheology and Shape Retention of Powder Injection Molding (PIM) Feedstock, World Congress 2014, Powder Metallurgy Proceedings, 2014, Orlando, USA.

B.N. Mukund, T.S. Shivashankar, M. Sachin, Metal Injection Molding of Stainless steels for surface finishing Applications, PowderMet 2015, Conference Proceedings, 2015, San Diego, California, USA.

B.N. Mukund, T.S. Shivashankar, Influence of powder packing characteristics on

MIM component, PM China 2017, Conference Proceedings, 2017, Shanghai, China.

B.N. Mukund, T.S. Shivashankar, Effect of powder particle parameters and its influence in Metal Injection Molding (MIM), PM China 2018, Conference Proceedings, 2018, Shanghai, China.

B.N. Mukund, T.S. Shivashankar, Rheological and mechanical properties of gas and water atomized SS 17-4PH feedstock used in Metal Injection Molding (MIM), World Congress on Powder Metallurgy 2018, Congress Proceedings, 2018, Beijing, China.

B.N. Mukund, T.S. Shivashankar, M. Sachin, Rheological and mechanical properties of super Co-400 alloy in Metal Injection Molding (MIM), 5th International conference on Powder Metallurgy in Asia, 2019, Pune, India.

B.N. Mukund, Sinter based AM – Large scale industrial adoption of Binder Jet Printing (BJT), Workshop on sinter-based Additive Manufacturing-2022, 2022, IFAM, Bremen, Germany.

B.N. Mukund, J. Holla, Binder jet metal printing -status report, international conference on Advanced manufacturing and technology (ICAM-2023), ASTM international, 2023, Washington D.C, USA.

Role of Powder Characteristics in Metal Injection Molding Process

Úloha morfologie kovových prášků v procesu jejich zpracování vstřikováním

Doctoral Thesis Summary

Published by: Tomas Bata University in Zlín,
nám. T. G. Masaryka 5555, 760 01 Zlín.

Edition: published electronically

Typesetting by: Mukunda Bhimasena Rao Nagaraj, Ph.D.

This publication has not undergone any proofreading or editorial review.

Publication year: 2024

First Edition

ISBN 978-80-7678-251-8